catalysts

MDPI

Article

Theoretical Study on the Lewis Acidity of the Pristine AlF_3 and Cl-Doped α-AlF_3 Surfaces

Christian Becker [1,*], Thomas Braun [2] and Beate Paulus [1,*]

[1] Institut für Chemie und Biochemie, Freie Universität Berlin, Arnimallee 22, 14195 Berlin, Germany
[2] Institut für Chemie, Humboldt-Universität zu Berlin, Brook-Taylor-Straße 2, 12489 Berlin, Germany; thomas.braun@cms.hu-berlin.de
* Correspondence: c.becker@fu-berlin.de (C.B.); b.paulus@fu-berlin.de (B.P.)

Abstract: In the past two decades, metal fluorides have gained importance in the field of heterogenous catalysis of bond activation reaction, e.g., hydrofluorination. One of the most investigated metal fluorides is AlF_3. Together with its chlorine-doped analogon aluminiumchlorofluoride ($AlCl_xF_{3-x}$, x = 0.05–0.3; abbreviated ACF), it has attracted much attention due to its application in catalysis. Various surface models for α-AlF_3 and their chlorinated analogues (as representatives of amorphous ACF) are investigated with respect to their Lewis acidity of the active centres. First-principle density functional theory (DFT) methods with dispersion correction are used to determine the adsorption structure and energy of the probe molecules CO and NH_3. The corresponding vibrational frequency shift agrees well with the measured values. With this insight we predict the local structure of the active sites and can clarify the importance of secondary interactions to the local anionic surrounding of the catalytic site.

Keywords: AlF_3; Cl-doped α-AlF_3; ACF; CO; NH_3; adsorption; DFT calculations; frequency shifts

Citation: Becker, C.; Braun, T.; Paulus, B. Theoretical Study on the Lewis Acidity of the Pristine AlF_3 and Cl-Doped α-AlF_3 Surfaces. *Catalysts* **2021**, *11*, 565. https://doi.org/10.3390/catal11050565

Received: 9 March 2021
Accepted: 25 April 2021
Published: 28 April 2021

1. Introduction

The vast majority of catalysts used on industrial scale are heterogenous catalyst with a high surface-to-volume ratio to increase the number of active sites. Very often, these catalysts are microcrystalline or even amorphous. This makes it difficult to gain knowledge on the electronic and structural properties of the active sites, a prerequisite to improve the performance of the catalyst.

In the past two decades, metal fluoride catalysts, especially high-surface aluminium fluoride, HS-AlF_3 and amorphous ACF (aluminiumchlorofluoride, $AlCl_xF_{3-x}$, $x = 0.05-0.3$), have shown high activity in several reactions such as C-H and C-F bond activation or hydroarylation reactions [1–6]. In selected reactions, these catalysts show comparable activity with the homogeneous catalyst SbF_5 [2]. To get more insight into the chemistry of these heterogenous catalysts, the Lewis acidity of the active sites, which describes their potential to bind to electron rich compounds, can be compared [7].

These metal fluoride catalysts show their catalytic behaviours only if they are synthesised as nanocrystalline material or like ACF only in its amorphous form. Therefore, it is far from trivial to get experimental characterization of these materials. One way to quantify the Lewis acidity is the adsorption of small molecules like CO and NH_3, where their lone pairs can bind to the positively charged catalytic centres. The adsorption of carbon monoxide (CO) and ammonia (NH_3) as probe molecules is an essential tool in the characterization of a surfaces' local properties [8–15]. Due to their adsorption at the active sites, the corresponding frequency shifts allow an estimation of Lewis-acidities, both experimentally and computationally [8–15]. For example, a large blue shift in the CO stretching vibration is associated with high Lewis acidity of an active, so-called coordinatively unsaturated site (CUS). Different frequency shifts can be associated with coordination numbers of the CUS on the surfaces [16].

In different experimental investigations, the Lewis acidity of milled α-AlF_3, β-AlF_3, high-surface AlF_3 (HS-AlF_3) and ACF were previously determined by the adsorption of CO and the corresponding IR spectra (see Table 1) [2,3,17,18]. Additionally Bailey et al. [19,20] performed theoretical studies at four- and fivefold coordinated aluminium centres of the β-AlF_3 (001), α-AlF_3-(0001) and α-AlF_3-(01$\bar{1}$2) surfaces with adsorbed CO, which show blue shifts comparable to the available experimental values. The measured frequencies were used as a basis for the classification of the Lewis acidic centres, by comparison of the frequency shift with the experimental CO frequency in the free molecule (2143 cm^{-1}) [3]. Whereas weakly physiosorbed CO shows nearly no shift (smaller than 10 cm^{-1}), very strong Lewis acidic centres can result in a blue shift up to ~80 cm^{-1} [3]. In this work, six different types of acidic centres were proposed, the most common ones being four- and fivefold coordinated aluminium centres, with fourfold coordinated ones assumed to be less Lewis-acidic than fivefold coordinated centres. This on the first glance counterintuitive behaviour is explained by the low accessibility of the fourfold active centre [14], due to the tetrahedral coordination environment. There are three types of fivefold coordinated aluminium centres on AlF_3-surfaces found, which differ by the number of terminal fluorine atoms [14]. Krahl and Kemnitz proposed that due to the higher electron withdrawing effect of bridging fluorine atoms, the electron pair acceptor strength of the aluminium centre decreases with the number of terminal fluorine atoms [14].

Table 1. Experimental CO frequencies on adsorption on AlF_3 and ACF. Frequency of the free CO is 2143 cm^{-1} [3]. Frequency shifts: ●: ~80 cm^{-1}, ○: 30–40 cm^{-1}.

Catalyst	β-AlF_3 [3]	HS-AlF_3 [3]	α-AlF_3 (Milled) [18] [1]	ACF [17]
wavenumber [cm^{-1}]	2220 ● 2180 ○ 2165 ○ 2145	2240 ● 2220 ● 2170 ○ 2150	2220 ● 2170 ○ 2150	2226 ● 2174 ○

[1] Values determined by us taken from Figure 6 in [18].

In the dissertation by Bailey [20], few surface structures of α- and β-AlF_3 were characterized via the adsorption of CO at the model surfaces. In this work, the adsorption of CO at the fourfold coordinated aluminium centers on the α-AlF_3-(0001) surface within a 2 × 1 cell and on the α-AlF_3-(01$\bar{1}$2) surface with a 1 × 1 and a $\sqrt{2} \times \sqrt{2}$ surface cell were investigated under the usage of the Crystal code with the B3LYP functional and the corresponding basis sets. The α-AlF_3-(0001) surface model shows adsorption energies between −0.16 to −0.30 eV with blue shifts of the CO stretch vibration of 78 and 88 cm^{-1}. For the α-AlF_3-(01$\bar{1}$2) surfaces, adsorption energies between −0.52 eV for the 1 × 1 and −0.21 eV for the $\sqrt{2} \times \sqrt{2}$ surface were found together with blue shifts of the CO stretch vibration between 72 and 87 cm^{-1}. For both surface models, the theoretical results are in the range of the experimental data [20]. Our previous investigations [21] have shown that the (01$\bar{1}$2) surface is quite high in energy and only another layer of fluorides and surface reconstruction stabilizes the α-AlF_3-(01$\bar{1}$2) surface. Locally, the structural motifs found by Bailey [20] and ours agree well, as proven by similar frequency shift obtained for CO. Contrary to the model of Bailey et al., the (0001) surface model used in this work shows threefold coordinated aluminium centers due to the usage of a different theoretical set-up and no additional fluorides [21].

For NH_3 as the probe molecule, there are three different vibrational frequencies that are affected by adsorption; the symmetric and asymmetric stretch modes in the range of 3300 cm^{-1} and a bending mode in the range of 1630 cm^{-1}. Different chemisorption modes for NH_3 on MgO [8,9] and ZnO [11] surfaces were characterized, but not much is known for the adsorption of NH_3 on metal fluoride surfaces. On these oxides, the adsorption of NH_3 on Lewis acidic CUS resulted in a blue shift of the asymmetric bending mode. This mode is most sensitive to the structural surrounding of the surface atoms, as it is highly affected by the formation of hydrogen bonds to the surface ions [9].

Furthermore, vibrational spectroscopy is a valuable experimental tool to characterize surfaces, and not much can be directly deduced on the local surrounding and possible secondary interactions to the anions. In this sense, first-principle investigations of different surface models of the heterogeous catalyst can help to elucidate the local properties.

Currently, there are only a few publications by Bailey et al. that characterize NH_3 adsorption on metal fluorides [15]. In related studies published by the same authors, the interactions with α- and β-AlF_3-surfaces were investigated with the focus on the adsorption of HF [22], H_2O [22] and CCl_2F_2 [23]. It can be assumed from the modelled structures by Bailey et al., that the binding motif of NH_3 is similar to the "upright" conformation of NH_3 on MgO surfaces [9], where the hydrogens can interact with the neighbouring terminal fluorine atoms of the surface. In the existing literature, only structural properties have been determined, and no frequencies for NH_3 on AlF_3 surfaces have been provided.

This paper covers studies on the adsorption of CO and NH_3 on different surface models of α-AlF_3 and Cl-doped α-AlF_3 under the usage of periodic DFT calculations, applying the PBE functional with D3-BJ dispersion correction. In earlier studies [21], different surfaces, which appear in the nano-crystal of the α-AlF_3, were characterized in detail and stable chloride-doped variants were proposed. The structural changes due to adsorption and the frequency shifts of the probe molecules are compared with the experimental results [3,17,18] of the corresponding fluorides. For the analysis of the electronic structure, the Bader charges for all surface models and density of states for selected ones are added to the Supplementary Materials. In none of the cases were interesting electronic contributions to binding found, therefore a more detailed analysis of the electronic structure with other methods like ELF or bond analysis on surfaces is not necessary [24]. Both are not straightforward methods with a plane-wave code used in this work.

The paper is organized as follows. After providing the computational details in Section 2, we describe the models in Section 3. The results are presented, discussed and compared with the experimental data in Section 4. The conclusion follows in Section 5.

2. Computational Details

All computations in this work were performed by applying the Vienna Ab Initio Simulation Package (VASP) [25–28]. The VASP code plane wave DFT with the PBE functional [29] was employed together with the plane wave (PAW) potentials [30] and the Γ-centered Monkhorst–Pack grid of size $6 \times 6 \times 2$ [31]. The plane waves cut-off criteria were set to 600 eV. In various ionic compounds, including various metal fluorides, PBE yields reasonable results [13,32–35]. Dispersion corrections were included via the D3-method [36] including BJ damping [37]. The vacuum size between the slabs was set to 25 Å. The van der Waals radius for D3-BJ corrections in the calculations was assigned to be 20 Å. The convergence criteria for the electronic self-consistent field loop was set to 1×10^{-5} eV for the first structure optimizations and were then refined to 1×10^{-7} eV for the frequency calculation. Additionally, the tetrahedron method with Blöchl corrections [38] was utilized. The force and stress tensors were calculated, and ions were relaxed for a fixed cell shape and volume using the conjugate gradient algorithm. The ionic relaxations were stopped when all forces acting on the ions were below 0.01 eV/Å for structural optimization and below 0.001 eV/Å for frequency calculations. The calculation of the frequencies was performed using the method of finite difference, as implemented in VASP. The Bader charge analysis was performed with the charge density grid method [39–41]. VESTA [42] was used for visualization. The same settings were used for the evaluation of our surface models [21].

3. Model

The most stable α-AlF_3 (space group $R\bar{3}c$) surfaces from our previous investigation [21] and their chlorinated variants were used as model surfaces to adsorb CO and NH_3. For the structure optimization, the probe molecules were placed at the fractional coordinates $x = 0.5$ and $y = 0.5$ of the 1×1 super cell of the selected surface with a distance of 3 Å to the highest surface atom, regardless of whether it was a fluoride or an aluminium ion. Additional

starting structures different to the one with which the first minimum structure was reached were applied, especially if multiple possible active centres are present. With this approach, a wider range of adsorption positions of certain surface models was included. Both probe molecules were placed in the C/N down position. To lower the computational cost, the six lower layers of the slab were fixed, and the upper layers (at least 6 layers) were optimised together with the probe molecules, including all possible degrees of freedom by "selective dynamics", as implemented in the VASP code. After the first structural optimization, the fine optimisation was done to perform the frequency calculation. Although different surface unit cells have different surface areas, in all cases, the adsorbed molecules are so far apart that their interaction energy is less than 5 meV and therefore below the accuracy that can be achieved with the current set-up.

For the comparison of the adsorbed to the non-adsorbed molecule, the free molecule was considered without the surface in a vacuum box of the same size as the 1×1 slab, with the same computational settings as the full system. For the free CO molecule, a C-O distance of 1.139 Å and a frequency of 2126 cm^{-1} was determined. This is a slightly longer distance and a slightly smaller frequency in comparison to the experimental values (1.131 Å, 2143 cm^{-1} [3,43]) but tolerable within the DFT framework that was applied.

The free NH_3 molecule shows N-H distances of 1.022 Å and a frequency of the bending vibration of 1624 cm^{-1}, which agree well with the experimental values of gaseous NH_3 (1.019 Å [44], 1628 cm^{-1} [11]). The full list of determined NH_3 frequencies can be found in Table S1 in the Supplementary Materials.

For the calculation of the adsorption energy, the differences between the adsorbed molecule on the surface and the separated systems was determined according to:

$$E_{ads} = E^{relaxed}_{surface+molecule} - E^{relaxed}_{surface} - E^{relaxed}_{molecule}$$

where the equilibrium structure (relaxed) is always used to evaluate the individual contributions. The corresponding frequency shift was calculated with

$$\nu_{Shift} = \nu_{adsorbed\ molecule} - \nu_{free\ molecule}$$

4. Results

In [21], we found, with the same computational methods, that α-AlF_3 is characterized by five different surfaces in vacuum. We could also show that replacing terminal and bridging fluorides by chloride results in no significant change in the relative stability of the surfaces. Therefore, the adsorption of the probe molecules was performed on the same surface cuts for both systems.

The most stable and most exposed (35–40%) $(01\bar{1}0)$ surface shows two tetrahedral coordinated aluminium sites. For the Cl-doped surface model, only one terminal fluoride was replaced by a chloride ion. The obtained structures of the probe molecules adsorbed to the α-AlF_3- and the Cl-doped α-AlF_3-$(01\bar{1}0)$ surface are depicted in Figure 1.

For CO, the Cl-doping affects the binding significantly. On the α-AlF_3-$(01\bar{1}0)$ surface, CO is physisorbed to the fourfold coordinated aluminium centre with a Al-C distance of 2.67 Å and an adsorption energy of −0.31 eV. The fluoride ions are far away from the adsorbed molecule; therefore, it is assumed that they have no influence on the binding. For the adsorbed CO, the bond distance with 1.134 Å is only 0.005 Å shorter as in the free molecule, but a medium-sized blue shift of the CO stretching frequency to 2165 cm^{-1} was determined.

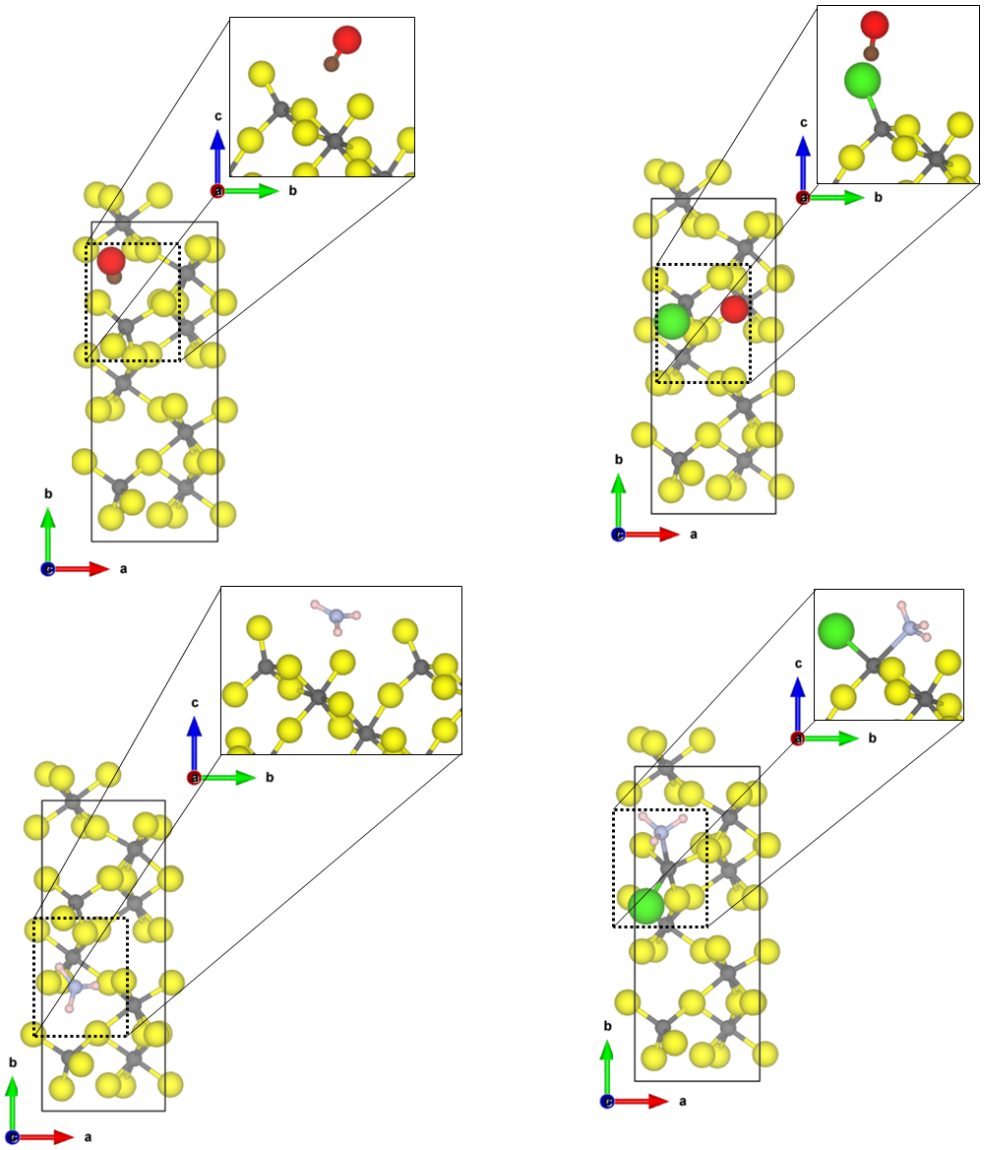

Figure 1. PBE-D3(BJ) optimized structures of the probe molecules CO (**upper row**) and NH_3 (**lower row**) on the 1 × 1 α-AlF_3- (**left**) and 1 × 1 Cl-doped α-AlF_3-(01$\bar{1}$0) surface; yellow = fluorine, grey = aluminium, brown = carbon, red = oxygen, blue = nitrogen, pink = hydrogen.

In contrast, for the Cl-doped α-AlF_3-(01$\bar{1}$0) surface, the CO adsorbs symmetrically between two terminal bound chlorine atoms with a Cl-C distance of 2.69 Å and an adsorption energy of −0.26 eV. The intramolecular distance in CO is 1.138 Å, which is in agreement with the assumed accuracy of the values for the free molecule. The larger Cl atoms hamper the approach of the CO to the aluminium site. The interaction of the CO molecule with the Cl atoms on this surface causes a slight red shift of the CO frequency to 2114 cm^{-1}.

The NH_3 molecule coordinates to three terminal fluorine atoms, with H···F hydrogen bond distances of 1.67 Å, 2.06 Å and 2.49 Å and the corresponding N-H bonds are changed by +0.014 Å, −0.004 Å and −0.007 Å, respectively. Comparing these distances to the intermolecular F-H···F-H distance of solid HF (1.53 Å [45]), we suggest that at least one hydrogen bond of medium strength is formed. The NH_3 molecule itself adopts a nearly planar conformation. For this interaction, an adsorption energy of −1.29 eV was found, which is characteristic for a chemisorption of the molecule; however, no covalent bonds are formed. Therefore, it can be assumed that each hydrogen bond add −0.43 eV, respectively, to the overall adsorption energy of the molecule. This is within the range of medium-sized hydrogen bonds in small molecules [46]. Unfortunately, it was not possible to converge

the structure with higher accuracy, a necessity for determining the vibrational frequencies. Different approaches, including the electronic minimization algorithms [47–49], ionic relaxation algorithms [50] and different starting points were used, however, with no success. These difficulties in reaching the convergence can be attributed to a very shallow potential energy surface, and for accurate results, the quantum nature of the hydrogens also has to be considered, which is far beyond the scope of this publication.

Whilst the CO on the Cl-doped α-AlF_3-(01$\bar{1}$0) surface cannot approach the CUS, NH_3 coordinates to the fourfold coordinated Al with a N-Al distance of 2.06 Å. One of the three hydrogen atoms forms a medium-strength hydrogen bond with a distance of 1.77 Å to a terminal fluoride of the surface, which elongates the NH bond by 0.002 Å compared to the free ammonia. The covalent bond formed between Al-N is strong enough (adsorption energy of −1.49 eV) to distort the tetrahedral enviroment to a trigonal pyramidal one. Surprisingly, the asymmetric bending frequency is only affected slightly with a small blue shift of 4 cm^{-1}.

Investigating now the second most abandoned (11$\bar{2}$2) surfaces, there are two differently coordinated aluminium sites (see Figure 2) at which CO can adsorb.

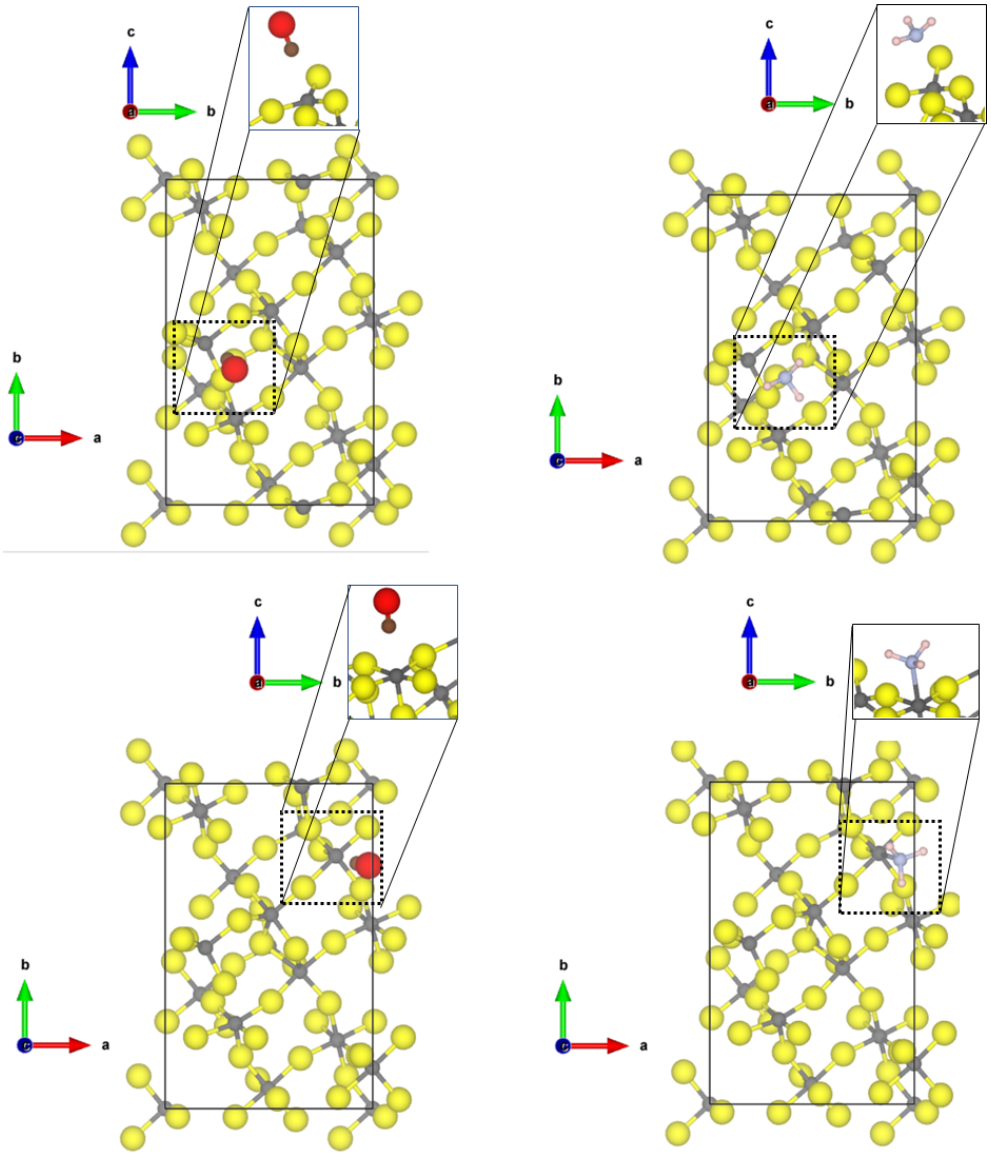

Figure 2. PBE-D3(BJ) optimized structures of the probe molecules CO (**upper row**) and NH_3 (**lower row**) on the 1 × 1 α-AlF_3-(11$\bar{2}$2) surface; left = tetragonal site; right = square-pyramidal site yellow = fluorine, grey = aluminium, brown = carbon, red = oxygen, blue = nitrogen, pink = hydrogen.

At the tetrahedral site, CO is bound with very similar adsorption energy (−0.30 eV, physisorption) as to the tetrahedral coordinated α-AlF_3-(01$\bar{1}$0) active site; however, a shorter Al-C distance of 2.40 Å and a larger blue shift to 2187 cm^{-1} was found. The adsorption of CO to the five-fold coordinated CUS is stronger compared to the fourfold coordinated one (adsorption energy of −0.60 eV), and a shorter Al-C distance of 2.24 Å was found, but the frequency is only shifted to 2158 cm^{-1}. In this case, there is no direct relation between adsorption strength and frequency shift. Despite the fact that the adsorption energy on the 5-fold CUS is doubled, the frequency shift is only half of the one on the fourfold CUS.

NH_3 also adsorbs on both available CUS of the α-AlF_3-(11$\bar{2}$2) surface. When bound to the fourfold CUS, the adsorption energy is in the range of physisorption (−0.48 eV) with a quite long Al-N distance (2.77 Å, see Figure 2) and a frequency shift of 7 cm^{-1}. The missing possibility of forming hydrogen bonds to the fluorides in this upright configuration (as found for the structure by Allouche et al. on MgO [9]) prevents a stronger binding. Therefore, all N-H distances are similar as in the free molecule, and the bending vibration is not affected. The situation is totally different at the 5-fold CUS. The NH_3 chemisorbs with an adsorption energy of −1.76 eV and an Al-N distance of 2.03 Å. Only weak hydrogen bonds are formed (H···F distances of 2.28 and 2.39 Å), and the bending frequency undergoes very little change (frequency shift of 8 cm^{-1}). The strong binding solely emerges from the chemical bond between Al-N. The determined Al-N bond length is only 0.1 Å longer than the experimental value found in crystalline AlN (1.89 Å [51]).

At the Cl-doped α-AlF_3-(11$\bar{2}$2), the CO molecule interacts with the tetragonal CUS with the terminal Cl atom (see Figure 3). The intramolecular CO distance undergoes very little change (1.137 Å), and an Al-C distance of 3.26 Å can be found. Due to the long Al-C distance, the adsorption energy is low (−0.22 eV). Cl-doping at the 5-fold CUS was found to be energetically not favourable [21]; therefore, no differences for the adsorption of the molecules are found compared to the equivalent CUS on α-AlF_3-(11$\bar{2}$2) (see Figure 2).

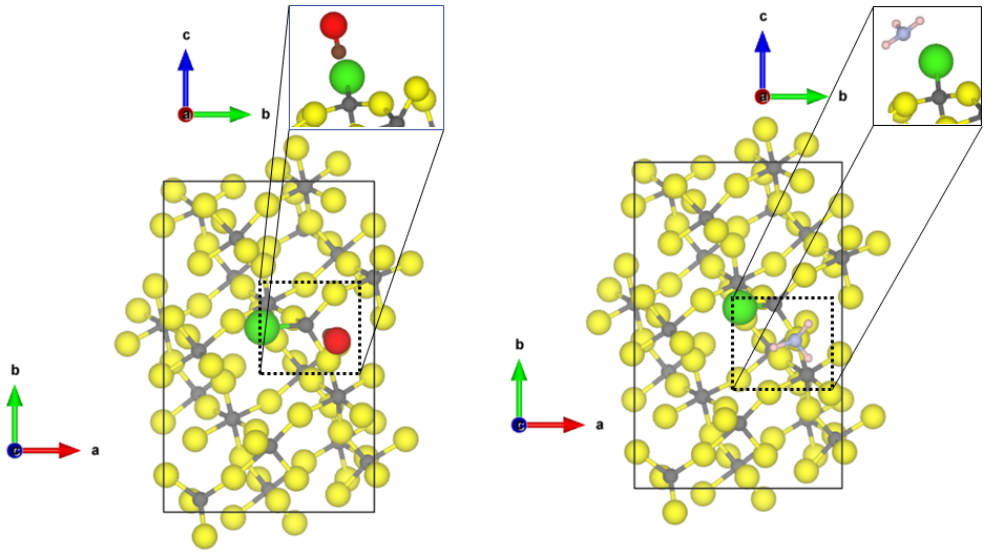

Figure 3. PBE-D3(BJ) optimized structures of the probe molecules CO (**left**) and NH_3 (**right**) on the 1 × 1 Cl-doped α-AlF_3-(11$\bar{2}$2) surface; yellow = fluorine, grey = aluminium, brown = carbon, red = oxygen, blue = nitrogen, pink = hydrogen.

For NH_3 at the tetragonal CUS bound to the Cl-doped α-AlF_3-(11$\bar{2}$2), a weak chemisorption with an adsorption energy of −0.75 eV and an Al-N distance of 2.61 Å is found. The molecule shows H···F/Cl distances between 2.7 Å and 2.9 Å. The conformation of the molecule is also comparable to the "upright" case found for the (01$\bar{1}$0) surface. Unfortunately, the structures of CO and NH_3 on the Cl-doped α-AlF_3-(11$\bar{2}$2) surface could not be optimized to the degree of accuracy necessary for the frequency analysis.

The third most abandoned surface in α-AlF_3 is the $(11\bar{2}0)$ surface; however, by Cl-doping its surface energy increases. This surface shows two 5-fold CUS with a square-pyramidal structure. Both CO and NH_3 adsorb at the CUS, independently of terminal or bridging substitution of fluorine with chlorine atoms (see Figure 4). For CO, a weak chemisorption (adsorption energy in the range of -0.7 eV) and Al-C distances of 2.19 Å were found. In all three cases, the intramolecular CO distance is around 1.132 Å and the frequencies were in the range of 2190 to 2205 cm^{-1} (blue shifts of 64 to 79 cm^{-1}).

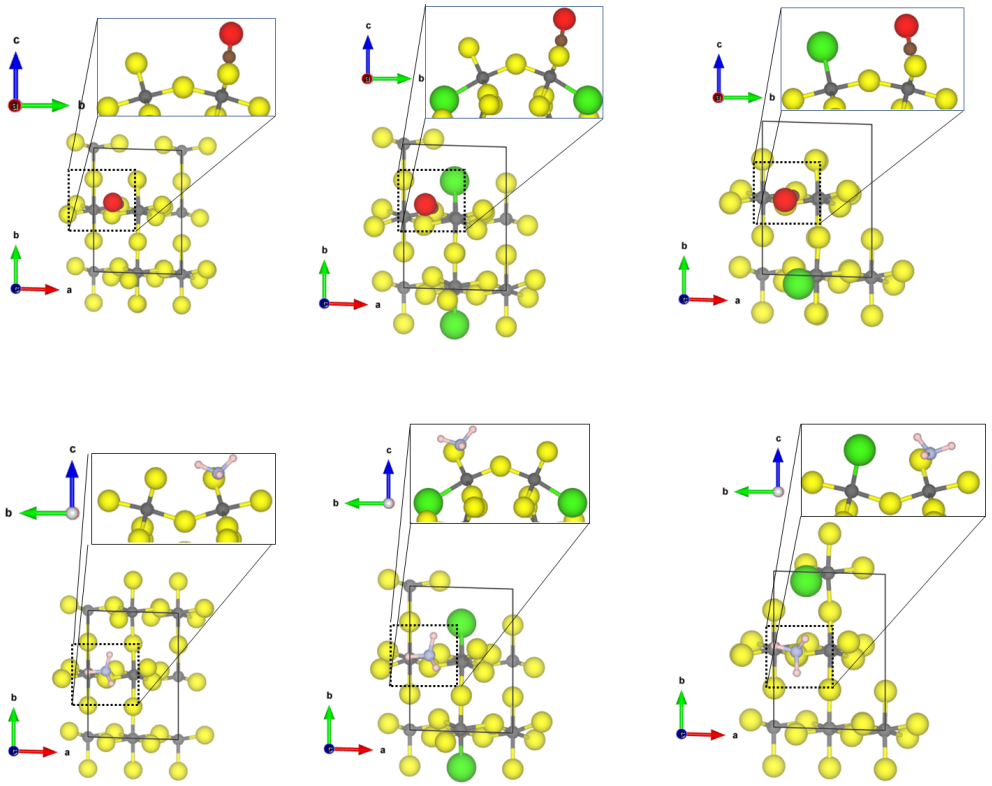

Figure 4. PBE-D3(BJ) optimized structure of the probe molecules CO (**upper row**) and NH_3 (**lower row**) on the α-AlF_3- (**left**) and Cl-doped α-AlF_3-$(11\bar{2}0)$ (**middle** and **right**) surfaces; yellow = fluorine, grey = aluminium, brown = carbon, red = oxygen, blue = nitrogen, pink = hydrogen.

NH_3 shows a weak chemisorption on the $(11\bar{2}0)$ surfaces (adsorption energy in the range of 0.9 eV), independently of the Cl-substitution. In all three cases, the Al-N bond length is about 2.3 Å. Alongside the weak chemical bond to Al, NH_3 forms a strong hydrogen bond to one fluoride at the surface (distance 1.74 Å) and another weak hydrogen bond with the distance of 2.14 Å. Although all NH distances were not changed by adsorption, owing to the quite strong hydrogen bond, the asymmetric bending mode is strongly affected with a blue shift in the range of 20 cm^{-1}.

For the less abundant (0001) and $(10\bar{1}2)$ surfaces, a highly undercoordinated threefold CUS structure occurs. This surface most likely only exists in high vacuum; however, it is interesting from a theoretical point of view. The binding structures of CO and NH_3 on the α-AlF_3 (0001) surface are shown in Figure 5.

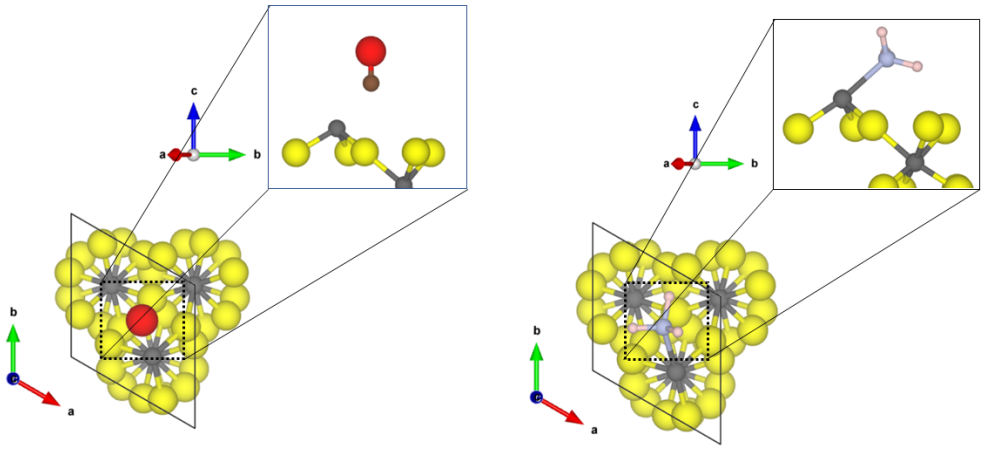

Figure 5. PBE-D3(BJ) optimized structures of the probe molecules CO (**left**) and NH_3 (**right**) on the α-AlF_3-(0001) surface; yellow = fluorine, green = chlorine, grey = aluminium, blue = nitrogen, pink = hydrogen, brown = carbon, red = oxygen.

Compared to the adsorption of CO to the fourfold and 5-fold CUS of the previous surfaces, a significant elongation of the CO bond length to 1.165 Å and a drastic red shift of the frequency by roughly 200 cm^{-1} upon coordination at the α-AlF_3-(0001) surface was found. This is an indication that an Al-C chemical bond is formed. The adsorption energy of CO on the threefold CUS (−1.01 eV) is somewhat higher than for the fourfold or fivefold ones, however, not as significant as one would expect from the large red shift. A significant amount of energy is necessary to elongate the CO bond, as the adsorption energy is referred to the free CO in equilibrium. By using the elongated CO bond as reference for the adsorption at the threefold CUS, the corresponding adsorption energy is lowered by 1.04 eV to −2.05 eV.

Furthermore, NH_3 adsorbs strongly on the threefold CUS of the (0001) surface, resulting in a short Al-N distance of 2.05 Å and a strong red shift (58 cm^{-1}) of the asymmetric bending mode. The adsorption energy of −1.25 eV (chemisorption) is not enhanced compared to fourfold and fivefold CUS. This is due to the missing hydrogen bonds to the fluorides (nearest H···F distance is 2.35 A) on the (0001) surface.

While the high surface energy prevents the (0001) surface from occuring in a Cl-doped α-AlF_3 crystal, the (10$\bar{1}$2) surface is stabilized by Cl-substitution [21] Therefore, only the latter surface is used for investigation of the effect of Cl substitution on the binding properties of CO and NH_3. Analysis of the threefold CUS for the adsorption of CO will be described here only since it adsorbs on the 5-fold CUS of the α-AlF_3-(10$\bar{1}$2) surface similar to the already discussed structures for the (11$\bar{2}$0) and (11$\bar{2}$2) surface (see Figure S1 in the Supplementary informations for the optimized structure).

The adsorption of CO and NH_3 at the threefold CUS of α-AlF_3-(10$\bar{1}$2) surface is very similar to the one found for the α-AlF_3-(0001) surface with a slightly larger Al-C distance and a weaker adsorption energy; however, the Cl-substitution has an effect on the binding. For the CO adsorption, two energetically similar adsorption sites were found, one similar to the case of the undoped surface (see Figure 6 middle) and one where the CO coordinates between the threefold CUS and the terminal chloride (see Figure 6 right). For these adsorption structures, the energies were determined to be between −0.54 for the α-AlF_3-(10$\bar{1}$2) surface and to −0.93 eV for the Cl-doped α-AlF_3-(10$\bar{1}$2) surface. Surprisingly, both show almost the same strong red shift (~200 cm^{-1}), although the structural binding motif is quite different.

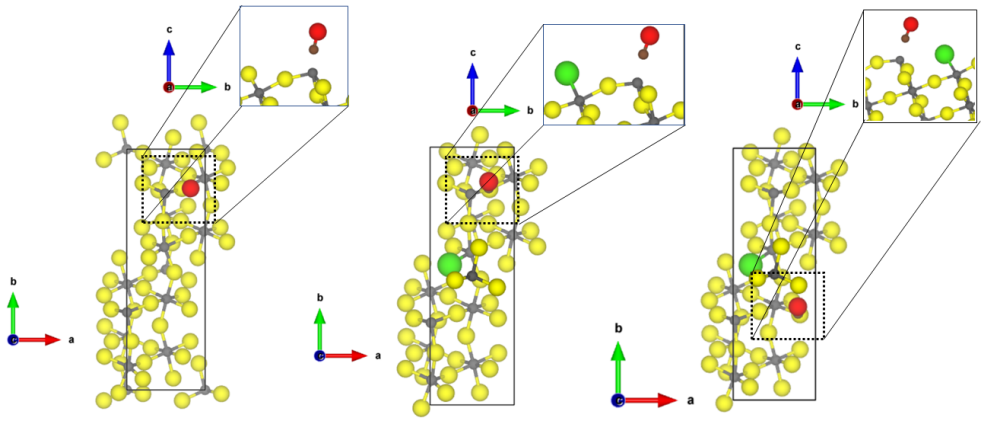

Figure 6. PBE-D3(BJ)-optimized structures of the probe molecule CO on the α-AlF_3- (**left**) and Cl-doped α-AlF_3-(10$\bar{1}$2) (**middle** and **right**) surface. yellow = fluorine, grey = aluminium, brown = carbon, red = oxygen.

The Cl substitution also has a beneficial effect on the NH_3 adsorption by lowering the adsorption energy by 0.4 eV and decreasing the Al-N bond length to 1.97 Å. However, in this case, the Cl is not involved in the binding. As previously stated, these changes are not correlated to a change in the frequency shift. In all cases, the NH_3 asymmetric binding mode is strongly red-shifted by about 45 cm^{-1}. The optimized structures of NH_3 on the (10$\bar{1}$2) surfaces can be found in the Supplementary Materials (Figures S2 and S3 for optimized structures).

5. Discussion

For comparison, the results for all adsorption sites on different surfaces are summarized in Table 2 for CO and Table 3 for NH_3.

Table 2. PBE-D3(BJ) results of the adsorption properties of CO on different α-AlF_3-surfaces and their Cl-substituted analogons. Frequency shifts: ●: ~80 cm^{-1}, ⋆: 50–60 cm^{-1}, ○: 30–40 cm^{-1}.

	Dist. C-O [Å]	**Dist. Al-C [Å]**	**E_{ads} [eV]**	**Freq. [cm^{-1}]**
CO	1.139	-	-	2126
Fivefold coordinated aluminium centre				
(11$\bar{2}$0)	1.130	2.19	-0.74	2205 ●
$(11\bar{2}0)_{Cl-term}$	1.132	2.19	−0.68	2190 ●
$(11\bar{2}0)_{Cl-bridge}$	1.131	2.19	−0.68	2201 ●
(11$\bar{2}$2)	1.132	2.24	−0.60	2158 ○
(10$\bar{1}$2)	1.123	2.24	−0.54	2177 ⋆
Fourfold coordinated aluminium centre				
(01$\bar{1}$0)	1.134	2.67	−0.31	2165 ○
$(01\bar{1}0)_{Cl-term}$	1.138	2.69 [1]	−0.26	2114
(11$\bar{2}$2)	1.132	2.40	−0.30	2187 ⋆
$(11\bar{2}2)_{Cl-term}$ [2]	1.137	3.26	−0.22	—
Threefold coordinated aluminium centre				
(0001)	1.165	2.08	−1.01	1925
(10$\bar{1}$2)	1.156	2.14	−0.59	1900
$(10\bar{1}2)_{Cl-term}$	1.156	2.00	−0.93	1938
	1.147	2.01	−0.90	1931

[1] The nearest atom is not an Al centre, but CO physiosorbs to two terminal Cl. [2] Accuracy for frequency analysis not achieved.

Table 3. PBE-D3(BJ) results of the adsorption properties of NH_3 bending vibration on different α-AlF_3-surfaces and their Cl-substituted analogion's. Experimental NH_3 bending vibration is ~1630 cm^{-1} [9]. Frequency shifts: •: ~20 cm^{-1}, ⋆: ~6 cm^{-1}.

	Dist. N-Al [Å]	**E_{ads} [eV]**	**Freq. [cm^{-1}]**
NH_3	-	-	1624
Fivefold coordinated aluminium centre			
$(11\bar{2}0)$	2.30	−0.89	1646 •
$(11\bar{2}0)_{Cl-term}$	2.31	−0.86	1641 •
$(11\bar{2}0)_{Cl-bridge}$	2.34	−0.82	1643 •
$(11\bar{2}2)$	2.03	−1.76	1632 ⋆
Fourfold coordinated aluminium centre			
$(01\bar{1}0)_{Cl-term}$	2.06	−1.49	1628 ⋆
$(01\bar{1}0)$[3]	—	−1.29	—
$(11\bar{2}2)_{Cl-term}$ [1]	2.61	−0.75	—
$(11\bar{2}2)$	2.77	−0.48	1631 ⋆
Threefold coordinated aluminium centre			
(0001)	2.05	−1.25	1566
$(10\bar{1}2)$	2.04	−0.95	1571
$(10\bar{1}2)_{Cl-term}$	1.97	−1.32	1569

[1] Accuracy for frequency analysis not achieved.

It can be observed that the aluminium centres with less sterical hindrance, such as threefold and fivefold coordinated centres, show usual more negative adsorption energies than fourfold coordinated centres. The highly symmetrical tetrahedral charge distribution around the aluminium site disfavours binding. Krahl et al. [14] has attributed this effect to a better electrostatic repulsions on the probe molecules. In the case of the Cl-doped α-AlF_3-$(01\bar{1}0)$ surface, the interaction formed with the NH_3 molecule is strong enough to undergo a reconstruction of the tetrahedron, and a trigonal-bipyramidal structure is formed, which is stabilized with additional hydrogen bonds to the surface fluorides. This stabilizing effect cannot occur in the case of the CO adsorption due to missing hydrogen atoms.

Concerning the influence of Cl-doping (comparing Cl-doped α-AlF_3 and corresponding α-AlF_3 aluminium sites) only small to negligible effects can be found for the adsorption of CO. It can be seen that the shielding of the surface by chlorine atoms is higher than the shielding by the fluorine atoms due to the more extended electron density, and therefore the binding is slightly reduced for the Cl-doped α-AlF_3 sites. For NH_3, however, the effect is weakened by the possibility of the molecule to form additional hydrogen bonds to the surface, which results in a additional stabilitation.

Regarding the frequency shift of the probe molecules adsorbed to the different coordinated aluminium centres, the molecules adsorbed on the unsaturated threefold coordinated aluminium centres show a large red shift. Due to the high binding affinity of the threefold coordinated aluminium centers a saturation with oxygen, water or other compounds of the realistic catalytic mixture would occur. Additionally, the abundance of the surfaces, where the threefold CUS occur, is below 12% for α-AlF_3 and 3% for Cl-doped α-AlF_3 [21]. Therefore the results would be only apply for special designed high-vacuum surface science experiments.

In constrast, the fourfold and fivefold coordinated aluminium centres are very stable and occur on many different surface cuts with high probability. For the CO stretching vibration, a significant blue shift, from 32 cm^{-1} to 79 cm^{-1}, was observed. Furthermore, the NH_3 bending vibration is blue-shifted by 4 cm^{-1} to 22 cm^{-1}. The CO blue shifts are in good agreement with the experimental results [2,3,17,18]. Additionally the adsorption energies for CO at the fourfold coordinated centres are in good agreement with the theoretical results of Bailey et al. [20]. According to the classification of Krahl et al. [3], weak, medium and strong Lewis acidic centres can be also found within our models. α-AlF_3-$(11\bar{2}0)$ and

the Cl-doped variants show strong Lewis acidic centres with frequency shifts between 64 and 79 cm^{-1} (see Table 2). With the same abundance, we find medium Lewis acidic centres on the α-AlF_3-(11$\bar{2}$2) and α-AlF_3-(10$\bar{1}$2) (frequency shifts between 52 and 62 cm^{-1}) and surfaces with frequency shifts of 32 cm^{-1} and 39 cm^{-1}, which correspond to weak Lewis acidic centres.

Cl-doping only yields small changes in the frequency shifts of the CO molecules. Therefore, it is likely that the same structural properties of the active sites in α-AlF_3 and Cl-doped α-AlF_3 occur. Because no electronic influence and nearly no effect on the local structure of the Cl-doping at α-AlF_3 surfaces on the adsorption of the probe molecules can be found, we assume that the experimentally measured activity in the ACF is due to its higher amorphicity and therefore due to a higher number of active sites. Besides the structural and vibrational analysis of the surface models, Bader charges and projected density of states for the chlorinated α-AlF_3-(01$\bar{1}$0) surface are also provided in the Supplementary Materials.

Additionally, the results of the investigations agree well with the statement of Krahl et al. [14], that the coordination number of the metal atom of a catalytic active site alone is not enough to determine the Lewis acid strength. For example, the fivefold coordinated aluminium centres show CO frequency shifts in a range of 2158 cm^{-1} to 2205 cm^{-1}, including weak, medium and strong Lewis acidic centres. The main difference between these active centres, shown by our calculations, is the explicit surrounding of the aluminium sites with different numbers of μ_1 or μ_2-F/Cl atoms.

Furthermore, for NH_3, different adsorption energies can be found for aluminium centres with the same coordination numbers. A range of adsorption energies from -0.48 to -1.76 eV was found independent of whether NH_3 binds to five-, four- and threefold coordinated aluminium centres. In comparison to the results of Bailey et al. [15], our calculations show adsorption energies that are somewhat decreased for the fivefold CUS. Due to the fact that the model of Bailey et al. does not include fourfold coordinated sites for the adsorption of ammonia, no comparison to this study can be made. Additionally, the H$\cdots$F distances of NH_3 to surface fluorines are within the range determined by Bailey et al. [15]. The maximum adsorption energy of -2.0 eV determined by Bailey et al. [15] cannot be observed within our calculations, this can be due to different surface models used or different functionals. Nevertheless, the two computational studies agree well.

6. Conclusions

DFT-based first principle calculations elucidate the structural and energetic properties of various surfaces occurring in nanoscopic aluminium fluoride-based materials. This study focused on the vibrational analysis of the probe molecules CO and NH_3 adsorbed on various $AlF_{3-x}Cl_x$ model systems, where $x = 0.15$, to improve the knowledge of the Lewis acidity of the catalytic sites in amorphous ACF. Additionally, the adsorption structures of the probe molecules are presented alongside the corresponding adsorption energies. It could be confirmed that the highest shielding against adsorption of CO molecules can be reached for tetragonal coordinated aluminium centres. In addition, it was confirmed that the Lewis acidity not only is based on the coordination number of the aluminium atom, but also depends on the surrounding μ_1 or μ_2-F/Cl atoms, which can build additional interactions to the probe molecules. Comparison of chlorinated and unchlorinated aluminium centres showed that, due to the chlorine doping, the shielding of the surface aluminium centre towards the coordination of CO/NH_3 is increased, if no additional interactions from the adsorbant to the surface, such as hydrogen bonds, can be formed. It can be expected that with the related decreased Lewis acidity for these chlorinated aluminium centres, the catalytic activity of the Cl-doped α-AlF_3 surfaces would also decrease, especially if steric and electronic effects dominate the catalytic processes. In contrast, Cl-doping yields a higher amorphicity of the catalyst and therefore a higher number of active sites. We can conclude that the Cl-doping has nearly no electronic effect and only small influences on the local structure, so the high catalytic activity of ACF probably has an macroscopic

origin, e.g., the high amorphicity, which influences the number of active sites and/or their accessibility. However, due to the overall good agreement between the theoretical and experimental results, we are confident that our structural models resemble the most common active sites in the amorphous systems ACF.

Supplementary Materials: The following are available at https://www.mdpi.com/2073-4344/11/5/565/s1. Figure S1: Optimized structure of the probe molecule CO on the fivefold coordinated center of the α-AlF_3-(10$\bar{1}$2) surface, Figure S2: Optimized structure of the probe molecule NH3 on the threefold coordinated center of the chlorinated (left) and unchlorinated (right) α-AlF_3-(10$\bar{1}$2) surface, Figure S3 Projected Density of states of CO adsorbed to the terminal chlorinated α-AlF_3-(01$\bar{1}$0) surface, Figure S4: Projected Density of states of the terminal chlorinated α-AlF_3-(01$\bar{1}$0) surface, Table S1: Summary of NH_3 vibrations on different α-AlF_3-surfaces and their Cl-substituted analogons, Table S2: Summary of atomic charges of adsorption sides at different α-AlF_3-surfaces and their Cl-substituted analogons along with the adsorbed molecules, Table S3: Summary of atomic charges of adsorption sides at different α-AlF_3-surfaces and their Cl-substituted analogons along with the adsorbed molecules.

Author Contributions: Conceptualization, B.P.; methodology, B.P. and C.B.; software, C.B.; validation, B.P., T.B. and C.B.; formal analysis, C.B.; investigation, C.B.; resources, B.P.; data curation, C.B.; writing—original draft preparation, C.B.; writing—review and editing, B.P., T.B. and C.B.; visualization, C.B.; supervision, B.P.; project administration, B.P.; funding acquisition, B.P. All authors have read and agreed to the published version of the manuscript.

Funding: The publication of this article was funded by Freie Universität Berlin.

Data Availability Statement: The data presented in this study are available in https://www.mdpi.com/2073-4344/11/5/565. Additional related data, especially the xyz-coordinates of the optimized structures are available on request from the corresponding author.

Acknowledgments: This project was funded by the Deutsche Forschungsgemeinschaft (DFG, German Research Foundation) Project-ID 387284271 SFB 1349. Gefördert durch die Deutsche Forschungsgemeinschaft (DFG)—Projektnummer 387284271—SFB 1349. Additionaly, we thank the North-German Supercomputing Alliance (Norddeutscher Verbund zur Förderung des Hoch- und Höchstleistungsrechnens HLRN) and the Zentraleinrichtung für Datenverarbeitung (ZEDAT) at the Freie Universität Berlin for computational ressources.

Conflicts of Interest: The authors declare no conflict of interest.

Abbreviations

The following abbreviations are used in this manuscript:

ACF	aluminiumchlorofluoride
CO	carbon monoxide
CUS	coordinatively unsaturated site
D3-BJ	D3 disperion correction with Becke-Johnson damping
DFT	density functional theory
HS-AlF_3	"high-surface" aluminiumtrifluoride
NH_3	ammonia
PBE	Perdew-Burke-Ernzerhof functional
VASP	Vienna ab initio simulation package

References

1. Calvo, B.; Wuttke, J.; Braun, T.; Kemnitz, E. Heterogeneous Catalytic Hydroarylation of Olefins at a Nanoscopic Aluminum Chlorofluoride. *ChemCatChem* **2016**, *8*, 1945–1950. [CrossRef]
2. Calvo, B.; Braun, T.; Kemnitz, E. Hydrogen/Deuterium-Exchange Reactions of Methane with Aromatics and Cyclohexane Catalyzed by a Nanoscopic Aluminum Chlorofluoride. *ChemCatChem* **2018**, *10*, 403–406. [CrossRef]
3. Krahl, T.; Vimont, A.; Eltanany, G.; Daturi, M.; Kemnitz, E. Determination of the Acidity of High Surface AlF_3 by IR Spectroscopy of Adsorbed CO Probe Molecules. *J. Phys. Chem. C* **2007**, *111*, 18317–18325. [CrossRef]
4. Krahl, T. Amorphes Aluminiumchlorofluorid und-Bromofluorid—Die Stärksten Bekannten Festen Lewis-Säuren. Ph.D. Thesis, Humboldt-Universität zu Berlin, Mathematisch-Naturwissenschaftliche Fakultät I, Berlin, Germany, 2005. [CrossRef]

5. Kemnitz, E.; Menz, D.H. Fluorinated metal oxides and metal fluorides as heterogeneous catalysts. *Prog. Solid State Chem.* **1998**, *26*, 97–153. [CrossRef]
6. Kervarec, M.C.; Marshall, C.P.; Braun, T.; Kemnitz, E. Selective dehydrofluorination of 2-chloro-1,1,1,2-tetrafluoropropane (HCFC-244bb) to 2-chloro-3,3,3-trifluoropropene (HFO-1233xf) using nanoscopic aluminium fluoride catalysts at mild conditions. *J. Fluor. Chem.* **2019**, *221*, 61–65. [CrossRef]
7. Muller, P. Glossary of terms used in physical organic chemistry (IUPAC Recommendations 1994). *Pure Appl. Chem.* **2009**, *66*, 1077–1184. [CrossRef]
8. Tench, A.J.; Giles, D. Infra-red study of the adsorption of ammonia on MgO. *J. Chem. Soc. Faraday Trans. 1* **1972**, *68*, 193–196. [CrossRef]
9. Allouche, A.; Corà, F.; Girardet, C. Vibrational infrared spectrum of NH3 adsorbed on MgO(100). I. Ab initio calculations. *Chem. Phys.* **1995**, *201*, 59–71. [CrossRef]
10. Fogash, K.B.; Yaluris, G.; González, M.R.; Ouraipryvan, P.; Ward, D.A.; Ko, E.I.; Dumesic, J.A. Characterization and selective poisoning of acid sites on sulfated zirconia. *Catal. Lett.* **1995**, *32*, 241–251. [CrossRef]
11. Morimoto, T.; Yanai, H.; Nagao, M. Infrared spectra of ammonia adsorbed on zinc oxide. *J. Phys. Chem.* **1976**, *80*, 471–475. [CrossRef]
12. Cant, N.W.; Little, L.H. An infrared study of the adsorption of ammonia on porous vycor glass. *Can. J. Chem.* **1964**, *42*, 802–809. [CrossRef]
13. Li, X.; Paier, J.; Sauer, J.; Mirabella, F.; Zaki, E.; Ivars-Barcelo, F.; Shaikhutdinov, S.; Freund, H.J. Surface Termination of Fe_3O_4(111) Films Studied by CO Adsorption Revisited. *J. Phys. Chem. B* **2018**, *122*, 527–533. [CrossRef] [PubMed]
14. Krahl, T.; Kemnitz, E. Aluminium fluoride—The strongest solid Lewis acid: structure and reactivity. *Catal. Sci. Technol.* **2017**, *7*, 773–796. [CrossRef]
15. Bailey, C.L.; Wander, A.; Mukhopadhyay, S.; Searle, B.G.; Harrison, N.M. Characterization of Lewis acid sites on the (100) surface of β-AlF_3: Ab initio calculations of NH_3 adsorption. *J. Phys. Chem.* **2008**, *128*, 224703. [CrossRef] [PubMed]
16. Kemnitz, E. Nanoscale metal fluorides: A new class of heterogeneous catalysts. *Catal. Sci. Technol.* **2015**, *5*, 786–806. [CrossRef]
17. Calvo, B.; Marshall, C.P.; Krahl, T.; Kröhnert, J.; Trunschke, A.; Scholz, G.; Braun, T.; Kemnitz, E. Comparative study of the strongest solid Lewis acids known: ACF and HS-AlF_3. *Dalton Trans.* **2018**, *47*, 16461–16473. [CrossRef] [PubMed]
18. Scholz, G.; König, R.; Petersen, J.; Angelow, B.; Doerfel, I.; Kemnitz, E. Mechanical Activation of α-AlF_3: Changes in Structure and Reactivity. *Chem. Mater.* **2008**, *20*, 5406–5413. [CrossRef]
19. Bailey, C.L.; Mukhopadhyay, S.; Wander, A.; Searle, B.G.; Harrison, N.M. First principles characterisation of aluminium trifluoride catalysts. *J. Phys. Conf. Ser.* **2008**, *117*, 012004. [CrossRef]
20. Bailey, C.L. Ab Initio Studies of Aluminium Halides. Ph.D. Thesis, Imperial College London, London, UK, 2009. [CrossRef]
21. Pandharkar, R.; Becker, C.; Budau, J.H.; Kaawar, Z.; Paulus, B. A Computational Study of AlF3 and ACF Surfaces. *Inorganics* **2018**, *6*, 124. [CrossRef]
22. Bailey, C.L.; Mukhopadhyay, S.; Wander, A.; Searle, B.G.; Harrison, N.M. Structure and Stability of α-AlF_3 Surfaces. *J. Phys. Chem. C* **2009**, *113*, 4976–4983. [CrossRef]
23. Bailey, C.L.; Mukhopadhyay, S.; Wander, A.; Searle, B.G.; Carr, J.M.; Harrison, N.M. Reactivity of the β-AlF_3(100) surface: defects, fluorine mobility and catalysis of the CCl_2F_2 dismutation reaction. *Phys. Chem. Chem. Phys.* **2010**, *12*, 6124–6134. [CrossRef] [PubMed]
24. Pecher, L.; Tonner, R. Deriving bonding concepts for molecules, surfaces, and solids with energy decomposition analysis for extended systems. *WIREs Comput. Mol. Sci.* **2019**, *9*, e1401. [CrossRef]
25. Kresse, G.; Hafner, J. Ab initio molecular dynamics for liquid metals. *Phys. Rev. B* **1993**, *47*, 558–561. [CrossRef] [PubMed]
26. Kresse, G.; Hafner, J. Ab initio molecular-dynamics simulation of the liquid-metal–amorphous-semiconductor transition in germanium. *Phys. Rev. B* **1994**, *49*, 14251–14269. [CrossRef] [PubMed]
27. Kresse, G.; Furthmüller, J. Efficiency of ab initio total energy calculations for metals and semiconductors using a plane-wave basis set. *Comput. Mater. Sci.* **1996**, *6*, 15–50. [CrossRef]
28. Kresse, G.; Furthmüller, J. Efficient iterative schemes for ab initio total-energy calculations using a plane-wave basis set. *Phys. Rev. B* **1996**, *54*, 11169–11186. [CrossRef]
29. Perdew, J.P.; Burke, K.; Ernzerhof, M. Generalized Gradient Approximation Made Simple. *Phys. Rev. Lett.* **1996**, *77*, 3865–3868. [CrossRef]
30. Kresse, G.; Joubert, D. From ultrasoft pseudopotentials to the projector augmented-wave method. *Phys. Rev. B* **1999**, *59*, 1758–1775. [CrossRef]
31. Monkhorst, H.J.; Pack, J.D. Special points for Brillouin-zone integrations. *Phys. Rev. B* **1976**, *13*, 5188–5192. [CrossRef]
32. Wirth, J.; Schacht, J.; Saalfrank, P.; Paulus, B. Fluorination of the Hydroxylated α-Al_2O_3 (0001) and Its Implications for Water Adsorption: A Theoretical Study. *J. Phys. Chem. C* **2016**, *120*, 9713–9718. [CrossRef]
33. Budau, J.H.; Paulus, B.; Steenbergen, K.G. Theoretical investigation of the crystal structure of AlOF. *Chem. Phys.* **2017**, *491*, 112–117. [CrossRef]
34. Vandichel, M.; Biswas, S.; Leus, K.; Paier, J.; Sauer, J. Catalytic Performance of Vanadium MIL-47 and Linker-Substituted Variants in the Oxidation of Cyclohexene: A Combined Theoretical and Experimental Approach. *ChemPlusChem* **2014**, *79*, 1183–1197. [CrossRef]

35. Kaawar, Z.; Müller, C.; Paulus, B. Theoretical investigations of the CO adsorption on ZnF_2 surfaces. *Surf. Sci.* **2017**, *656*, 48–53. [CrossRef]
36. Grimme, S.; Antony, J.; Ehrlich, S.; Krieg, H. A consistent and accurate ab initio parametrization of density functional dispersion correction (DFT-D) for the 94 elements H-Pu. *J. Chem. Phys.* **2010**, *132*, 154104. [CrossRef] [PubMed]
37. Becke, A.D.; Johnson, E.R. A density-functional model of the dispersion interaction. *J. Chem. Phys.* **2005**, *123*, 154101. [CrossRef] [PubMed]
38. Bloch, F. Über die Quantenmechanik der Elektronen in Kristallgittern. *Z. Phys.* **1929**, *52*, 555–600. [CrossRef]
39. Tang, W.; Sanville, E.; Henkelman, G. A grid-based Bader analysis algorithm without lattice bias. *J. Phys. Condens. Matter* **2009**, *21*, 84204–84210. [CrossRef] [PubMed]
40. Sanville, E.; Kenny, S.D.; Smith, R.; Henkelman, G. Improved grid-based algorithm for Bader charge allocation. *J. Comp. Chem.* **2007**, *28*, 899–908. [CrossRef]
41. Henkelman, G.; Arnaldsson, A.; Jónsson, H. A fast and robust algorithm for Bader decomposition of charge density. *Comp. Mat. Sci.* **2006**, *36*, 354–360. [CrossRef]
42. Momma, K.; Izumi, F. It VESTA3 for three-dimensional visualization of crystal, volumetric and morphology data. *J. Appl. Cryst.* **2011**, *44*, 1272–1276. [CrossRef]
43. Glockler, G. Carbon–Oxygen Bond Energies and Bond Distances. *J. Phys. Chem.* **1958**, *62*, 1049–1054. [CrossRef]
44. Kuchitsu, K.; Guillory, J.P.; Bartell, L.S. Electron-Diffraction Study of Ammonia and Deuteroammonia. *J. Chem. Phys.* **1968**, *49*, 2488–2493. [CrossRef]
45. Johnson, M.W.; Sándor, E.; Arzi, E. The crystal structure of deuterium fluoride. *Acta Crystallogr. Sect. B* **1975**, *31*, 1998–2003. [CrossRef]
46. Steiner, T. The Hydrogen Bond in the Solid State. *Angew. Chem. Int. Ed.* **2002**, *41*, 48–76. [CrossRef]
47. Davidson, E.R. The iterative calculation of a few of the lowest eigenvalues and corresponding eigenvectors of large real-symmetric matrices. *J. Comput. Phys.* **1975**, *17*, 87–94. [CrossRef]
48. Pulay, P. Convergence acceleration of iterative sequences. The case of scf iteration. *Chem. Phys. Lett.* **1980**, *73*, 393–398. [CrossRef]
49. Wood, D.M.; Zunger, A. A new method for diagonalising large matrices. *J. Phys. A Math. Gen.* **1985**, *18*, 1343–1359. [CrossRef]
50. Press, W.H.; Flannery, B.P.; Teukolsky, S.A.; Vetterling, W.T. *Numerical Recipes—The Art of Scientific Computing*; Cambridge University Press: Cambridge, UK, 1986; ISBN 9780521880688.
51. Ott, H. Das Gitter des Aluminiumnitrids (AlN). *Z. Phys.* **1924**, *22*, 201–214. [CrossRef]